future pharmacology

MDPI

Article

Intranasally Delivered Mesenchymal Stem Cells Reverses Prodromal Non-Motor Deficits and Nigral Loss in a Parkinson's Disease Mouse Model

Soung Hee Moon [1], Young Eun Huh [2,*] and Hyun Jin Choi [1,*]

[1] College of Pharmacy and Institute of Pharmaceutical Sciences, CHA University, Pocheon 11160, Gyeonggi-do, Republic of Korea; anstjdgml1@chauniv.ac.kr
[2] Department of Neurology, CHA Bundang Medical Center, CHA University, Seongnam 13488, Gyeonggi-do, Republic of Korea
* Correspondence: ye.huh@chamc.co.kr (Y.E.H.); hjchoi3@cha.ac.kr (H.J.C.); Tel.: +82-31-881-7168 (H.J.C.)

Abstract

Background/Objectives: Parkinson's disease (PD) is a progressive neurodegenerative disorder characterized by the loss of dopaminergic neurons in the substantia nigra (SN). Because current therapeutics have limited efficacy once PD is fully developed, it is crucial to start disease-modifying interventions during the prodromal stage of PD. In the present study, we aimed to evaluate whether intranasally delivered human umbilical cord mesenchymal stem cells (hUC-MSCs) have an efficacy in the rotenone-induced prodromal PD-like phenotype mouse model. Methods: To produce the prodromal PD mouse model, C57BL/6 mice were treated with intraperitoneal (i.p.) rotenone for 1 or 2 weeks. hUC-MSCs or PBS were delivered intranasally for 1 or 2 weeks with rotenone injection. We subsequently performed behavioral assessments to evaluate motor and non-motor features, followed by pathological analyses of the mouse brains. Results: Intranasal administration of hUC-MSCs restored motor performance and protected dopaminergic neurons in the SN of mice treated with rotenone for 2 weeks. In the 1-week rotenone mice, hUC-MSCs treatment ameliorated depressive-like behaviors and attenuated olfactory dysfunction. Furthermore, intranasal hUC-MSC treatment suppressed the accumulation of protein aggregates in the brains of mice, which is associated with enhanced autophagic function, as indicated by increased LC3B and normalization of LAMP2A protein expression. Conclusions: Our data demonstrate that intranasal administration of hUC-MSCs improves non-motor symptoms at early time points and attenuates progression to nigrostriatal loss and motor deficits in the rotenone-induced PD mouse model. These findings support the potential of a non-invasive, prodromal-stage intervention to modulate early pathological progression in PD.

Keywords: Parkinson's disease; human umbilical cord mesenchymal stem cells; non-motor symptoms; autophagy; protein aggregation; intranasal administration; rotenone

Academic Editor: Ali Zarrabi

Received: 28 November 2025
Revised: 5 January 2026
Accepted: 13 January 2026
Published: 2 February 2026

1. Introduction

Parkinson's disease (PD) is a neurodegenerative disorder characterized by the progressive loss of dopaminergic neurons in the substantia nigra (SN) [1]. Clinically, PD is diagnosed based on motor symptoms such as rigidity, tremor, and bradykinesia that typically appear after more than 60% of nigral neurons have degenerated [2]. Several non-motor signs, including olfactory dysfunction, sleep disturbances, depression, and anxiety, often predate the onset of motor deficits, which enhances their potential as prodromal markers of

PD [3,4]. Many studies aimed at developing disease-modifying therapies are now targeting individuals at the prodromal stage, where disease burden is less extensive, to maximize therapeutic efficacy [5–7].

The pathogenesis of PD involves various cellular processes, including oxidative stress, neuroinflammation, mitochondrial dysfunction, and abnormal protein aggregation [8,9]. Notably, the accumulation of abnormal protein aggregates, including Lewy bodies, in dopaminergic neurons is a pathological hallmark of PD [10]. Lewy bodies are intracellular inclusions composed primarily of misfolded α-synuclein, a protein that plays a critical role in synaptic function and neurotransmitter release [11]. Based on these pathological characteristics, increasing the clearance of aggregated proteins, particularly via autophagy induction, has recently emerged as a promising therapeutic strategy for PD. Although autophagy dysfunction is primarily documented in the later (full-blown) stage of PD, modulating this pathway at the prodromal stage may help restrain early disease progression.

Rotenone is widely used as a neurotoxin to establish experimental animal models of PD [12,13]. As a lipophilic mitochondrial complex I inhibitor, rotenone induces α-synuclein aggregation and Lewy body–like inclusions, more faithfully recapitulating key pathological features of PD than other neurotoxin-induced models [14]. Short-term rotenone administration is particularly suitable for reproducing prodromal symptoms [15,16].

The blood–brain barrier (BBB) protects the brain from external substances [17,18] but poses a significant obstacle for treating central nervous system (CNS) disorders, including PD [19]. The BBB tightly regulates the entry of molecules essential for brain function, such as glucose and essential amino acids, through specific transporters [20,21]. Unlike peripheral capillaries, the paracellular spaces between endothelial cells in brain capillaries are nearly nonexistent due to the tight junctions that seal BBB endothelial cells together [22,23]. To overcome this barrier, drug-delivery approaches, including nanocarriers or chemical modification, have been developed to enhance CNS penetration [24,25]. Furthermore, strategies that bypass the BBB entirely and directly target the brain have also been explored [26,27]. In this context, cell therapy has attracted attention, not only for its secretome and immunomodulatory functions [28–30] but also because extracellular vesicles (EVs) released by cells can cross the BBB to some extent or modulate its function indirectly [31–33]. Intranasal administration has emerged as a promising CNS drug-delivery route because it bypasses the BBB via neural pathways connecting the olfactory epithelium to the brain parenchyma [34–36]. Several animal studies have demonstrated that intranasally administered cells or cell-derived vesicles rapidly reach the brain along the olfactory and trigeminal nerve pathways, allowing repeated administration without invasive procedures [37–39]. Furthermore, intranasal administration has been proposed to reduce off-target systemic distribution and enhance local therapeutic effects by providing direct access to the brain without passing through systemic circulation [40–42].

Mesenchymal stem cells derived from the human umbilical cord (hUC-MSCs) exhibit higher proliferative capacity, delayed cellular senescence, and lower donor-to-donor variability compared with bone marrow- or adipose tissue-derived MSCs [43] hUC-MSCs display low immunogenicity due to minimal expression of major histocompatibility complex (MHC) class II molecules and possess a robust secretory profile enriched in anti-inflammatory cytokines, neurotrophic factors, and EVs [44–46]. Administration of hUC-MSCs has been reported to ameliorate motor deficits and attenuates neurodegeneration in the 1-methyl-4-phenyl-1,2,3,6-tetrahydropyridine (MPTP)-induced PD mouse model [47]. Indeed, MSCs have been detected in the brain as early as one day post-administration and persist for at least three weeks, suggesting the potential for sustained neuroprotective effects [48–51]. Despite prior evidence, whether MSCs can modulate early pathological changes in the prodromal stage remains unclear.

Building on these findings, the present study aimed to investigate whether non-invasive intranasal delivery of hUC-MSCs could alleviate non-motor symptoms during the prodromal-like stage of PD and improve motor function by protecting neurons in a rotenone-induced mouse model of PD. Furthermore, we examined whether these effects are associated with the attenuation of abnormal protein aggregation through autophagy modulation.

2. Materials and Methods

2.1. Antibodies and Reagents

Minimum essential medium α (α-MEM; 12571063) and fetal bovine serum (FBS; SH30919.03) were purchased from Gibco/Life Technologies (Carlsbad, CA, USA). Rotenone (R8875), dimethyl sulfoxide (D2650), hydrogen peroxide, 30 wt.% (216763), Triton X-100, for molecular biology (T8787), 3,3′-Diamino-benzidine tablets (DAB; D4793), FGF-4 (F8424), gentamicin (G1272), and heparin (H3149) were purchased from Sigma-Aldrich (St. Louis, MO, USA). The following antibodies were used: anti-tyrosine hydroxylase (anti-TH; ab112) and anti-ubiquitin (ab7254; both from Abcam; Cambridge, UK); anti-p62 (p0067; Sigma-Aldrich); anti-α-synuclein (GTX112799; Genetex; San Antonio, TX, USA); anti-LC3B (NB600-1384; Novus; St Charles, MO, USA); biotinylated anti-rabbit IgG (H + L; BA-1000), biotinylated anti-mouse IgG (H + L; BA-9200) (Vecta labs; Sydney, Australia). Paraformaldehyde (PFA; 4%; HP2031) was purchased from Biosesang (Seongnam, Republic of Korea), and Tissue-Tek O.C.T compound (4583) was from Sakura Finetek (Tokyo, Japan). The ABC kit (PK-6100) and hematoxylin QS (H3404) were obtained from Vector Laboratories (Newark, CA, USA).

2.2. Animals and Treatments

The animal experiments were performed in accordance with the Animal Research: Reporting of In Vivo Experiments (ARRIVE) guidelines and were approved by the CHA University Institutional Animal Care and Use Committee (IACUC; 230108). Eight-week-old male C57BL/6 mice (20–24 g) were purchased from Orient Bio (Seongnam, Republic of Korea). Mice were maintained at 22 °C, 50% humidity, and a 12 h light–dark cycle. Mice were housed in standard laboratory cages and had free access to food and water throughout the study. Rotenone was administered intraperitoneally (i.p.) once daily at a dose of 1 mg/kg for 1 and 2 weeks. Rotenone was suspended in 1% polyethylene glycol (PEG) with 0.2% DMSO. Control groups were injected with 1% PEG and 0.2% DMSO. hUC-MSCs (1×10^6/20 μL) were administered in each nostril three times a week [52,53]. To enhance nasal mucosal permeability, mice were pretreated intranasally with 5 μL of hyaluronidase (100 U; Sigma-Aldrich) in phosphate-buffered saline (PBS) 30 min before hUC-MSC treatment [54]. During intranasal administration, the mice were positioned with their abdomens and jaws upward, and this position was maintained for 3 min. The experimental timeline for the treatment with rotenone and hUC-MSCs is shown in Figure 1.

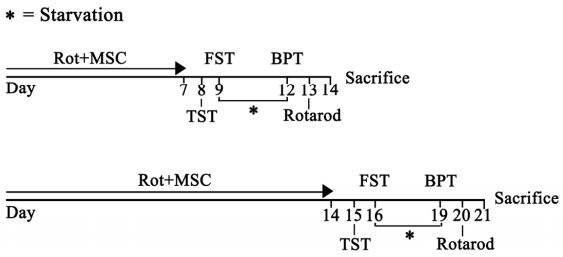

Figure 1. Experimental schedule for 1 and 2 weeks of rotenone treatment (1 mg/kg, i.p.) and intranasal hUC-MSCs administration (1×10^6 per mouse). Numbers indicate days after rotenone treatment. Buried pellet test, BPT; Forced swim test, FST; mesenchymal stem cells, MSC; Rotenone, Rot; Tail suspension test, TST.

2.3. Cell Culture

Human umbilical cord-derived MSCs were obtained from CHA Biotech (Seongnam, Republic of Korea). Cells were cultured in α-MEM supplemented with 10% FBS, 1 μg/mL heparin, 50 μg/mL gentamicin, and 25 ng/mL FGF-4 in 150 mm dishes and incubated at 37 °C under 5% CO_2.

2.4. Tail Suspension Test and Forced Swimming Test

To assess depressive-like behavior, we used the tail suspension (TST) and forced swimming (FST) tests [55]. For TST, adhesive tape was attached to the tail of each mouse, and the mice were suspended from a partitioned shelf to prevent visual contact for 6 min [56]. Behavior was recorded for the full 6 min, and immobility time was measured for 5 min, excluding the first min [57]. For the FST, mice were placed in a transparent cylindrical tank (30 × 10 cm in diameter) filled with warm water (27 °C, 20 cm in depth) [58]. The mice were video recorded for 6 min, and the immobility time was measured for 5 min, excluding the first min [59]. Immobility time was defined as the period during which the mouse remained floating without movement, except that required to keep its nose above water [60].

2.5. Buried Pellet Test (BPT) and Visual Pellet Test (VPT)

Before the BPT, mice were food-restricted for 2 days [61]. Each mouse was individually placed in a cage and habituated for 1 h to adapt to the new bedding. Afterward, one piece of cereal (1 g) was buried along the cage wall at a depth of 1 cm beneath the bedding and concealed from view [62]. The mouse was subsequently placed on the side opposite to the pellet, and the latency to uncover and start eating was recorded using a stopwatch [63]. The VPT was performed in the same manner, except that the pellet was placed on top of the bedding to ensure visibility. This test enabled assessment of motivation and motor ability independent of olfactory cues.

2.6. Rotarod Test

A rotarod treadmill (JD-A-07MA5, Jeung Do Bio & Plant Co., Ltd., Seoul, Republic of Korea) was used to assess motor function. Mice completed one training and three test sessions, each separated by at least 20 min. During training, mice were required to maintain their balance on a rotating rod for 3 min at a fixed speed of 4 rpm. If the mice fell, they were returned to the rod until the session was completed [64]. For testing, the rotation speed was increased from 4 to 40 rpm at an acceleration of 10 rpm/min [65]. The latency to fall was recorded for each mouse. Each session ended when the mice fell from the rod or remained there for 5 min.

2.7. Perfusion and Immunohistochemistry

Mice were deeply anesthetized with a 1:1 mixture of Zoletil and Rompun (50 mg/kg, i.p.) and were perfused slowly through the aorta with 50 mL of 1X PBS, followed by 4% PFA [66]. After perfusion, brains were quickly removed and post-fixed in 4% PFA for 24 h. Brains were incubated in 15% sucrose solution for 24 h, then in 30% sucrose solution for an additional 24 h [67]. Brain tissues were embedded in Tissu-Tek O.C.T. compound, frozen at −80 °C for at least 2 h, and then coronally sectioned at 20-μm thickness using a cryostat [68]. Tissue sections were mounted on slides after 10 min of washing in 0.05 M PBS, three times. For antigen retrieval, brain sections were immersed in Tris-EDTA buffer for 3 min to expose antigenic sites [69]. Sections were permeabilized and blocked for 30 min at room temperature in 1% bovine serum albumin (BSA, BSAS 0.1) (Bovogen Biological; Keilor East, Australia)/1.5% normal goat serum (NGS, 01-6201; Thermo Fisher

Scientific; Waltham, MA, USA)/0.3% hydrogen peroxide/0.2% Triton X-100/0.05M PBS. Brain sections were incubated overnight at 4 °C in 0.05 M PBS containing 1.5% normal goat serum with the following primary antibodies: rabbit polyclonal anti-TH (1:200); mouse monoclonal anti-ubiquitin (1:200); rabbit polyclonal anti-p62 (1:200); rabbit polyclonal anti-LC3B (1:200); and rabbit polyclonal anti-α-synuclein (1:300). The next day, sections were incubated for 1 h at room temperature with biotinylated anti-rabbit or anti-mouse IgG (H + L) secondary antibodies. After several washes, immunoreactivity was visualized using DAB staining [70].

2.8. Immunofluorescence

Immunofluorescence was performed as described previously [71]. Brain sections were incubated overnight at 4 °C in 0.05 M PBS containing 2% normal donkey serum and 1% BSA with rat polyclonal anti-LAMP2A primary antibodies (1:800). Sections were incubated with donkey anti-rat IgG Alexa Fluor 647 (Invitrogen, Eugene, OR, USA; Cat# A78947) secondary antibodies for 1 h at room temperature, followed by incubation with 4′,6-diamidino-2-phenylindole for 10 min. The images were captured using a digital slide scanner (Zeiss, Jena, Germany). All paired images in the figures were acquired under identical gain and offset settings. Spot intensities were measured using ImageJ software (version 1.54p).

2.9. Statistical Analysis

For quantitative analysis, three fields per experimental condition were acquired from each coverslip, and the mean was used for statistical analysis. All analyses were performed blinded. All data are expressed as the mean ± the standard error of the mean. Statistical significance for multiple comparisons was assessed using one-way analysis of variance followed by Sidak's multiple comparisons test in Prism (GraphPad Software, version 10, La Jolla, CA, USA).

3. Results

3.1. hUC-MSCs Attenuate the Motor Deficit and Protect SN Dopaminergic Neurons in Rotenone-Induced PD Mice

To examine rotenone-induced dopaminergic neuronal loss in the SN, and whether these pathological changes are ameliorated by intranasally delivered hUC-MSCs, we first assessed immunostaining in both brain hemispheres of rotenone-treated mice. A 1-week rotenone treatment did not significantly reduce TH immunoreactivity in the SN or impair motor performance in the rotarod test (Figures 2 and 3A). However, after 2 weeks of rotenone-alone treatment, TH immunoreactivity was significantly reduced, which was markedly restored in the group that received hUC-MSCs with rotenone (Figure 2). Additionally, the rotarod test showed that mice that received both rotenone and hUC-MSCs for 2 weeks exhibited improved motor performance compared to those from the rotenone-only group (Figure 3B). Although 2-week rotenone-treated mice showed a tendency toward reduced rotarod performance that did not reach statistical significance, hUC-MSC co-treatment significantly enhanced motor performance compared with the rotenone-only treated group. Together, these findings indicate that 2 weeks of rotenone treatment in mice results in early pathological alterations without significant motor deficits, and that these pathological changes can be ameliorated by intranasally delivered hUC-MSCs.

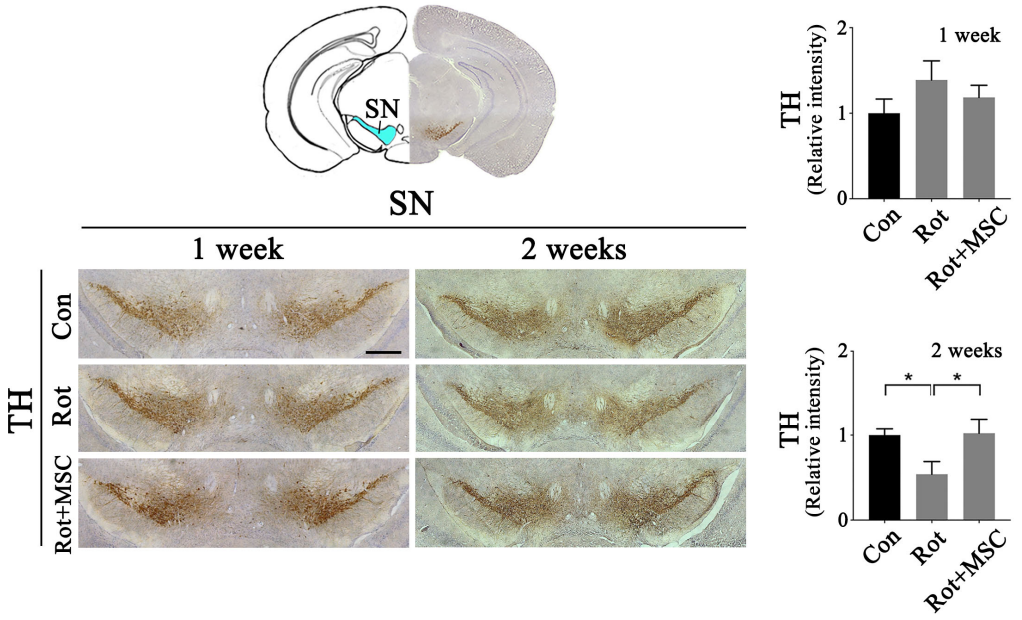

Figure 2. Assessment of survival of dopaminergic neurons in the rotenone-induced mouse model of PD intranasally administered with hUC-MSCs. Immunohistochemistry analysis of TH-positive cells in the SN (**left panel**) and densitometric quantification (**right panel**) (n = 4). TH-positive regions are shown in brown, and the nuclei are counterstained in blue. Error bars indicate the standard error of the mean. * $p < 0.05$. Scale bars = 500 μm. Control, Con; Mesenchymal stem cells, MSC; Rotenone, Rot; Substantia nigra, SN; Tyrosine hydroxylase, TH.

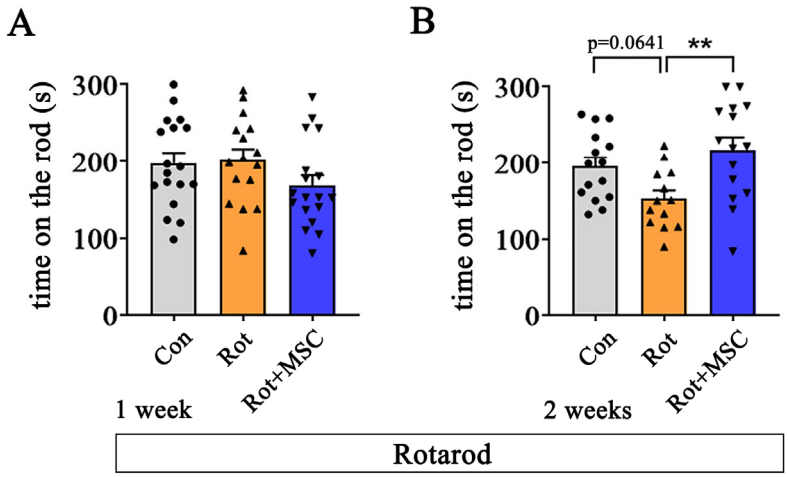

Figure 3. Evaluation of motor performance in the rotenone-induced mouse model of PD following intranasal hUC-MSC administration. Effect of hUC-MSCs administration on motor function in the 1- (**A**) and 2-week (**B**) rotenone-induced PD models (n = 13–18). ● (gray bar), ▲ (orange bar), and ▼ (blue bar) indicate individual animals in the control, rotenone, and rotenone plus hUC-MSCs groups, respectively. Error bars indicate the standard error of the mean. ** $p < 0.01$. Control, Con; Mesenchymal stem cells, MSC; Rotenone, Rot.

3.2. hUC-MSCs Alleviate Non-Motor Symptoms During the Early Stage of Rotenone-Induced PD Mice

To determine whether rotenone reproduces prodromal-like non-motor symptoms of PD, we evaluated olfactory function and depressive-like behaviors in mice treated with rotenone for 1 or 2 weeks. In the 1-week rotenone-treated group, immobility time was significantly increased in the FST (Figure 4B, left panel), whereas a trend toward increased immobility, but not significant, was observed in the TST (Figure 4A, left panel), indicat-

ing depressive-like behavior characteristic of the prodromal PD-like phenotype. This increase in immobility was significantly reduced by hUC-MSC treatment (Figure 4A,B, left panel). However, no significant changes were observed in the 2-week rotenone-treated mice (Figure 4A,B, right panel). Furthermore, the VPT was performed to determine whether visual, motor, or cognitive deficits affected these behavioral results. No significant differences were observed in the 1- or 2-week hUC-MSC-administered groups (Figure 4C). In the BPT, olfactory ability tended to improve after hUC-MSC administration in both 1- and 2-week rotenone-treated groups (Figure 4D). Together, these results indicate that 1 week of rotenone exposure reproduces prodromal-like non-motor features, which are attenuated by intranasal administration of hUC-MSC.

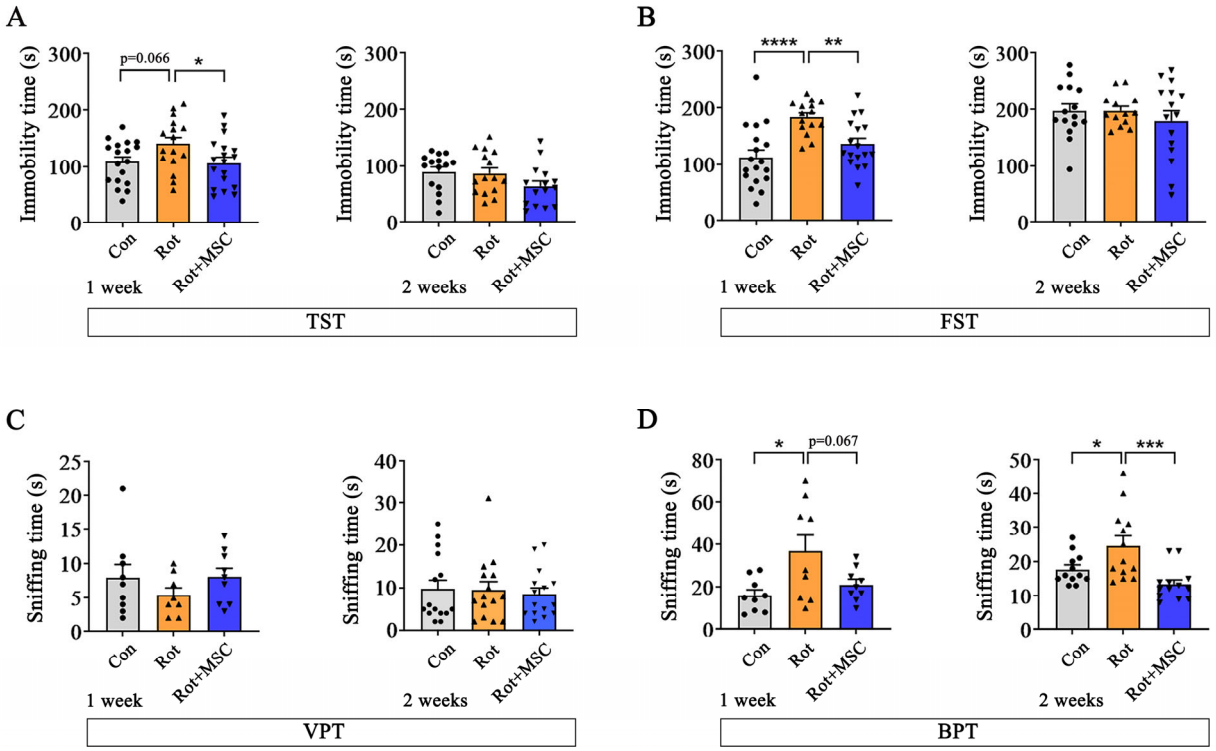

Figure 4. Analysis of non-motor symptoms following hUC-MSC intranasal administration. Immobility time (s) of mice in the TST (**A**) and FST (**B**) after intranasal administration of hUC-MSCs with rotenone for 1 and 2 weeks (n = 13–18). To determine whether visual, motor, or cognitive deficits affected the results, the VPT was performed (**C**) (n = 8–9). BPT results on changes in olfactory function following the intranasal administration of hUC-MSCs (**D**) (n = 8–13). ● (gray bar), ▲ (orange bar), and ▼ (blue bar) indicate individual animals in the control, rotenone, and rotenone plus hUC-MSCs groups, respectively. Error bars indicate the standard error of the mean. * $p < 0.05$, ** $p < 0.01$, *** $p < 0.001$, **** $p < 0.0001$. Buried pellet test, BPT; Control, Con; Forced swim test, FST; Mesenchymal stem cells, MSC; Rotenone, Rot; Tail suspension test, TST; Vertical pole test, VPT.

3.3. hUC-MSCs Attenuate Protein Aggregates in Early-Stage Rotenone-Induced PD Mice

Next, we investigated whether hUC-MSC-induced improvements in non-motor symptoms were accompanied by a reduction in abnormal protein aggregation in the brain. After 1 week of rotenone treatment, p62, α-synuclein, and ubiquitin (Ub) levels were significantly increased in the olfactory bulb (OB), and these increases were markedly attenuated by hUC-MSCs (Figure 5A). Quantitative analyses focused on the mitral cell layer (MCL) of the OB, a region particularly vulnerable to abnormal protein aggregation [72]. In the striatum, p62 and α-synuclein levels increased significantly following rotenone injection, while Ub showed a similar but non-significant trend (Figure 5B). Co-treatment with hUC-MSCs and rotenone significantly reduced the accumulation of these proteins compared with rotenone

alone (Figure 5B). In the SN, rotenone-induced increases in p62 and Ub immunoreactivity were significantly attenuated by hUC-MSC administration, restoring these protein levels to near those of the control group; in contrast, α-synuclein levels remained unchanged (Figure 5C).

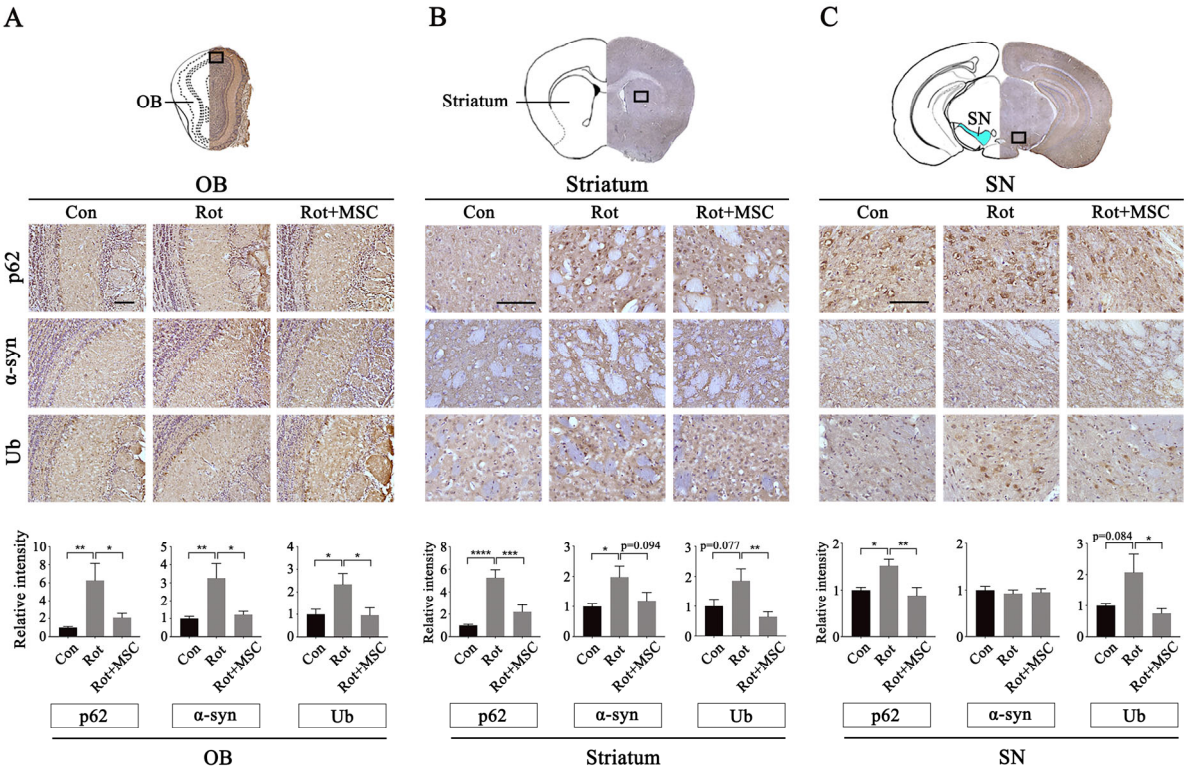

Figure 5. Changes in protein aggregation in the brain of rotenone-induced Parkinson's Disease (PD) mice after hUC-MSC administration. hUC-MSC administration reduced p62, α-syn, and Ub levels in the OB (**A**), striatum (**B**), and SN (**C**) of rotenone-treated 1-week mice. Quantification data are shown in the lower panels (**A**–**C**) (n = 12–15). p62, α-synuclein, and Ub are visualized in brown, and nuclei are counterstained in blue. Boxes indicate the regions selected for higher-magnification images, and solid lines denote scale bars. Error bars indicate the standard error of the mean. * $p < 0.05$, ** $p < 0.01$, *** $p < 0.001$, **** $p < 0.0001$. Scale bars = 100 µm. α-Synuclein, α-syn; Control, Con; Mesenchymal stem cells, MSC; Olfactory bulb, OB; Rotenone, Rot; Substantia nigra, SN; Ubiquitin, Ub.

3.4. hUC-MSCs Modulate Autophagy and Reverse Rotenone-Induced Changes in TH Immunoreactivity in the OB

As the OB showed the most prominent reduction in protein aggregates following hUC-MSC administration and because OB pathology is linked to early olfactory dysfunction, we next investigated whether this effect involved regulation of autophagy-related signaling pathways [73]. Autophagy-related markers were analyzed within the MCL, where protein aggregation appeared the earliest and mitral cells were densely distributed. LC3B, a marker of autophagosome formation, was significantly increased in the brains of rotenone-treated mice and was further upregulated in mice co-treated with rotenone and hUC-MSCs (Figure 6A). In contrast, LAMP2A immunoreactivity was reduced in the rotenone-treated group but recovered in mice treated with both rotenone and hUC-MSCs (Figure 6B), suggesting the restoration of lysosomal function. In the OB, TH immunoreactivity was significantly elevated in mice treated with rotenone alone for 1 week, whereas hUC-MSC administration normalized TH levels to those observed in the control group (Figure 7). Increased TH expression in the OB has been reported as a pathological feature associated with olfactory dysfunction in the prodromal PD-like phenotype [74]; therefore, this result

suggests a possible link between hUC-MSC effects and recovery of olfactory function (Figure 4D).

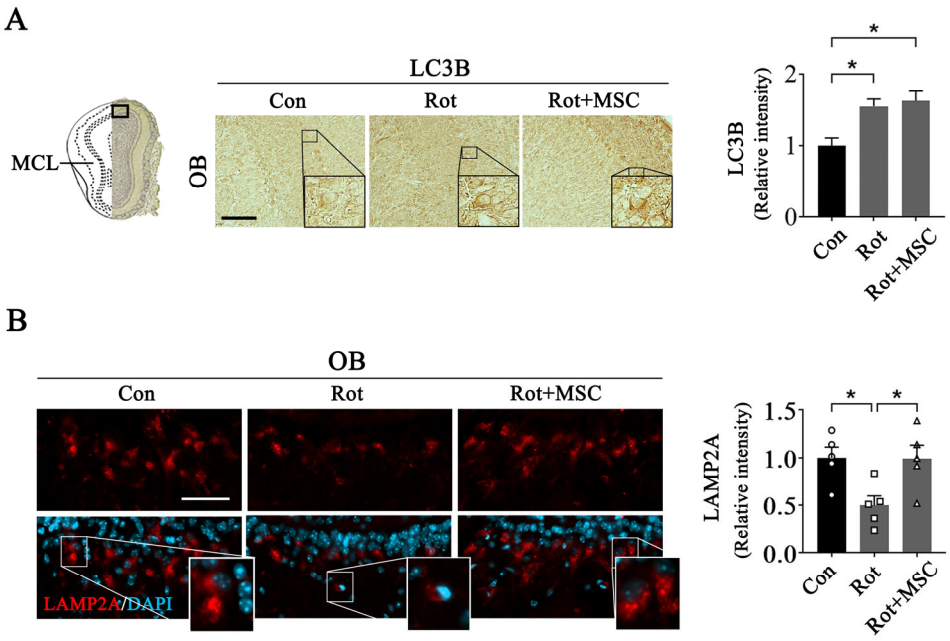

Figure 6. hUC-MSC intranasal administration activates impaired autophagic flux. Immunohistochemical analysis and quantification of LC3B levels in the OB (**A**, **left panel**) and their densitometric quantification (**A**, **right panel**) (n = 4–8). Brown signals indicate LC3B, and the nuclei are counterstained blue. Scale bars = 200 μm. Recovery of LAMP2A (red) levels in OB following hUC-MSC administration, as shown by immunofluorescence analysis (**B**, **left panel**) and quantitative data (**B**, **right panel**): LAMP2A levels decreased by rotenone were recovered by hUC-MSC administration. (n = 5). ○, □, △ indicate individual animals in the control, rotenone, and rotenone plus hUC-MSCs groups, respectively. Boxes indicate the regions selected for higher-magnification images, and solid lines denote scale bars. Scale bars = 50 μm. Error bars indicate the standard error of the mean. * $p < 0.05$. Control, Con; Mesenchymal stem cells, MSC; Mitral cell layer, MCL; Olfactory bulb, OB; Rotenone, Rot.

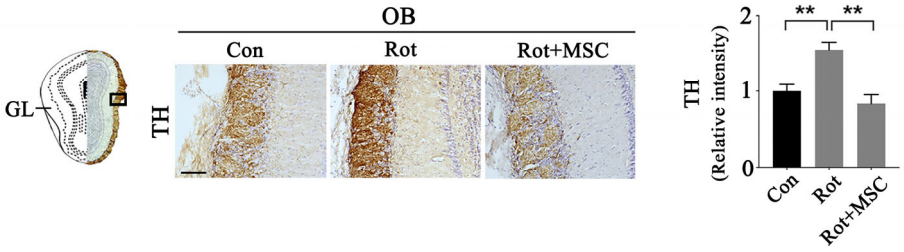

Figure 7. hUC-MSC intranasal administration restores TH expression to normal levels. Immunoreactivity of TH-positive cells in OB (**left panel**) and their quantitative analysis (**right panel**) (n = 10). Boxes indicate the regions selected for higher-magnification images, and solid lines denote scale bars. Scale bars = 50 μm. Error bars indicate the standard error of the mean. ** $p < 0.001$. Control, Con; Glomerular layer, GL; Mesenchymal stem cells, MSC; Olfactory bulb, OB; Rotenone, Rot; Tyrosine hydroxylase, TH.

4. Discussion

This study demonstrates that the intranasal administration of hUC-MSCs attenuates motor impairments and improves early non-motor symptoms, including depressive-like behavior and olfactory dysfunction, in a rotenone-induced mouse model of PD. Furthermore, hUC-MSC treatment reduced the accumulation of pathological protein aggregates.

These effects were supported by increased LC3B-II protein levels and normalization of LAMP2A expression, suggesting that hUC-MSCs may suppress disease progression by reactivating autophagy-related pathways during the early phase of PD.

Rotenone administration has been widely used to generate PD–like pathology, as it induces progressive dopaminergic neuronal loss in the SN and depletion of striatal dopamine. In facts, previous study showed that intraperitoneal administration of rotenone at a dose of 1 mg/kg resulted in a time-dependent decrease in the number of TH-positive neurons in the SN and dopamine content in the striatum from day 7 to day 21 [75]. Based on previous rotenone study, we would like to establish experimental conditions that reproduce early-stage PD-like pathology. In our study, a significant reduction in dopamine neurons in the SN was shown in mice treated with rotenone for 2 weeks. At this time point, motor performance showed a trend toward reduction, although the difference did not reach statistical significance (Figures 2 and 3). Clinically, substantial dopaminergic neuronal loss in the SN may occur without overt motor symptoms, which usually emerge only after 70–80% neuronal degeneration and marked striatal dopamine [76]. In this study, typical prodromal symptoms, such as depression and olfactory dysfunction, were clearly detected in the 1-week rotenone-treated group (Figure 4), accompanied by pathological changes that have been clinically reported in early PD [77,78], including abnormal protein accumulation (Figure 5) and increased TH-positive neurons in the OB (Figure 7). Although the degree of statistical significance varied depending on the behavioral experiment used (TST and FST), the overall behavioral pattern consistently indicated the emergence of characteristic non-motor symptoms of prodromal PD patients. The sensitivity of TST and FST in detecting depressive-like behavior can differ depending on experimental conditions and disease models [79]. Moreover, studies directly comparing the TST and FST have reported that corticosterone levels are significantly elevated during the FST, whereas no such increase is observed during the TST [80]. Together, these findings constitute a reasonable, clinically relevant model of PD, suggesting that our model is well-suited for investigating pathology and therapeutic interventions targeting the prodromal phase of PD.

We administered hUC-MSCs via the intranasal route, which is a noninvasive delivery strategy that has been shown to facilitate CNS access while minimizing systemic exposure [81]. Intranasally delivered MSCs or MSC-derived products can reach various brain regions, including the OB and midbrain, within hours to days after administration and may persist for several days, primarily exerting effects through paracrine mechanisms rather than long-term engraftment [37,82]. The dosing regimen used in the present study—administration of 1×10^6 hUC-MSCs three times per week—was selected based on prior preclinical studies demonstrating behavioral and neuropathological benefits without overt toxicity following repeated intranasal MSC delivery [37,83]. Although we did not directly assess hUC-MSC biodistribution or persistence in the brain in this study, accumulating evidence supports the notion that intranasally administered hUC-MSCs, or their secreted EVs, can exert biologically meaningful effects within the CNS [84,85].

Intranasally delivered hUC-MSCs ameliorated not only prodromal symptoms in the prodromal PD-like mice model (Figure 4) but also improved the underlying pathological alterations observed at the corresponding disease stage. In the 1 week rotenone model, hUC-MSC administration was found to be associated with attenuation of non-motor symptoms, accompanied by reduced abnormal protein accumulation (Figure 5) and normalization of region-specific pathological markers in the OB (Figure 6). Although these pathological assessments were performed at 1 week after rotenone treatment, suppression of protein aggregation is particularly relevant because protein accumulations are considered critical events that contribute to subsequent dopaminergic neurodegeneration in PD [86]. Modulation of early pathological processes may have downstream consequences for disease

progression; therefore, as per our results hUC-MSC-mediated improvement of early non-motor symptoms and associated pathology might contribute to longer-term regulation of disease-relevant neurodegenerative processes, supporting the therapeutic relevance of targeting early-stage PD pathology. Moreover, intranasal hUC-MSC treatment ameliorated brain pathology associated with PD. hUC-MSC increased TH-positive neurons in the OB (Figure 7), a compensatory mechanism that occurs rapidly in the early stages of PD [87,88]. Enhanced dopaminergic activity may inhibit olfactory signaling by suppressing synaptic transmission between olfactory receptor neurons and mitral cells [89,90]. Consistent with this observation, the number of TH-positive cells in the OB of PD patients with olfactory dysfunction have been found to be nearly twice than that of controls [74]. The findings from our study suggest that hUC-MSCs can counteract early pathological changes and prevent decline in olfactory function. In addition, hUC-MSCs significantly reduced abnormal protein accumulation in rotenone-treated mice by restoring impaired autophagic flux. Dysregulated autophagy is a major contributor to early PD-like pathology; our results indicate that hUC-MSCs help stabilize homeostatic protein degradation before irreversible neuronal loss occurs. This finding underscores the importance of early intervention in PD. Moreover, the intranasal route of hUC-MSC administration provides a clinically feasible and noninvasive approach for delivering these agents to the CNS.

Although hUC-MSC treatment ameliorated non-motor symptoms and improved the underlying pathological alterations, the precise mechanisms mediating these effects were not directly evaluated in the present study. Nevertheless, our data indicate that intranasal administration of hUC-MSC was associated with modulation of autophagy-related pathways. Notably, MSCs have been reported to exert context-dependent effects on autophagy, with several previous studies describing autophagy induction, inhibition, or enhanced autophagic turnover depending on experimental conditions, disease models, and cellular targets [91–93]. Under our experimental conditions, hUC-MSC treatment was accompanied by increased LC3 expression, normalization of LAMP2A levels, and a reduction in rotenone-induced protein accumulation. These coordinated changes are consistent with an overall enhancement of autophagy-related activity rather than an impaired degradation. While this interpretation remains associative, our findings support the possibility that hUC-MSC-mediated regulation of autophagy contributes to improved proteostasis and mitigation of early pathological processes in this model.

Whether the observed effects are mediated by direct actions of MSCs within the brain or indirectly through MSC-derived paracrine factors, particularly EVs, remain unclear. Evidence, however, suggests that the therapeutic effects of MSCs are largely mediated by their EVs [94–96]. MSC-derived EVs carry a diverse cargo of bioactive molecules, including microRNAs, proteins, lipids, and antioxidant enzymes, that can modulate neuroinflammation, oxidative stress, and cellular stress responses [97,98]. Furthermore, in models of neurodegenerative diseases, MSC-EVs have been shown to attenuate microglial activation, reduce pro-inflammatory cytokine production, and promote neuronal survival, even in the absence of detectable cell engraftment [84,99]. Therefore, EVs can readily cross biological barriers and diffuse within brain tissue, supporting their potential role as mediators of the observed neuroprotective and anti-inflammatory effects following intranasal MSC administration [100]. While direct evidence linking MSC-derived EVs to the effects observed in the present study is lacking, these findings suggest that EV-mediated mechanisms contribute, at least in part, to the modulation of early pathological processes in this prodromal PD model. In addition, although human-derived MSCs were administered in a xenogeneic setting, hUC-MSCs are generally considered to exhibit low immunogenicity. Repeated intranasal administration of human-derived MSCs for 4 weeks has been reported to not induce abnormalities in the brain or other major organs in mice [101]; however, some

reports have suggested the potential for a xenogeneic immune response [102]. Therefore, these drugs should be considered for temporary rather than long-term administration.

Our previous study demonstrated that administering trehalose in a rotenone-induced early PD-like phenotype model enhanced autophagy and improved both non-motor and motor symptoms [71]. The present study extends on these findings by providing novel evidence that hUC-MSCs can attenuate early pathological changes and non-motor symptoms of PD by normalizing autophagic activity. In contrast to prior studies focusing on the late motor phase of PD, our findings suggest a potential preventive role for early intervention during disease progression. This study evaluated the effect of hUC-MSC as an early intervention in the stage when initial pathological stress is formed; therefore, rotenone and hUC-MSC were administered simultaneously. However, in future studies, administering hUC-MSC after disease onset will be necessary to verify the long-term therapeutic effects of hUC-MSC. Overall, these results suggest that hUC-MSCs have preventive potential for early-stage PD-like phenotypes and may represent a novel approach to modifying disease progression.

5. Conclusions

Our findings indicate that intranasal administration of hUC-MSCs is associated with improvements in early non-motor symptoms and attenuation of early pathological changes in a rotenone-induced PD-like mouse model. These results support the feasibility of intranasal hUC-MSC delivery as a non-invasive approach for targeting early-stage PD pathology and justify further long-term and mechanistic investigations.

Author Contributions: Conceptualization: S.H.M. and H.J.C.; Methodology: S.H.M.; Investigation: S.H.M.; Data Curation: S.H.M.; Formal Analysis: S.H.M.; Validation: S.H.M.; Visualization: S.H.M.; Writing—Original Draft: S.H.M.; Writing—Review and Editing: H.J.C.; Supervision: H.J.C. and Y.E.H.; Funding Acquisition: Y.E.H. All authors had full access to all the data in the study and take responsibility for the integrity of the data and the accuracy of the data analysis. All authors have read and agreed to the published version of the manuscript.

Funding: This work was supported by the National Research Foundation of Korea (NRF) grants funded by the Korean government (MSIT) (NRF-2016M3A9E8941671 and RS-2024-00356889).

Institutional Review Board Statement: The animal study protocol was approved by the CHA University Institutional Animal Care and Use Committee (protocol code IACUC 230108 approved on 1 June 2023).

Informed Consent Statement: Not applicable.

Data Availability Statement: The raw data supporting the conclusions of this article will be made available by the authors on request.

Conflicts of Interest: The authors declare no personal or financial relationships that could have influenced the results of this study.

Abbreviations

α-MEM	Minimum Essential Medium Alpha
α-syn	α-Synuclein
ARRIVE	Animal Research: Reporting of In Vivo Experiments
BPT	Buried Pellet Test
BSA	Bovine Serum Albumin
Con	Control
DAB	3,3′-Diaminobenzidine
DMSO	Dimethyl Sulfoxide

FBS	Fetal Bovine Serum
FGF-4	Fibroblast Growth Factor-4
FST	Forced Swimming Test
GL	Glomerular Layer
hUC-MSC	Human Umbilical Cord Mesenchymal Stem Cell
i.p.	Intraperitoneal
IACUC	Institutional Animal Care and Use Committee
IgG	Immunoglobulin G
IHC	Immunohistochemistry
IF	Immunofluorescence
LC3B	Microtubule-Associated Protein 1A/1B-Light Chain 3B
LAMP2A	Lysosome-Associated Membrane Protein 2A
MCL	Mitral Cell Layer
OB	Olfactory Bulb
PBS	Phosphate-Buffered Saline
PD	Parkinson's Disease
PEG	Polyethylene Glycol
Rot	Rotenone
SEM	Standard Error of the Mean
SN	Substantia Nigra
TST	Tail Suspension Test
VPT	Visual Pellet Test

References

1. Paumier, K.L.; Sukoff Rizzo, S.J.; Berger, Z.; Chen, Y.; Gonzales, C.; Kaftan, E.; Li, L.; Lotarski, S.; Monaghan, M.; Shen, W.; et al. Behavioral characterization of A53T mice reveals early and late stage deficits related to Parkinson's disease. *PLoS ONE* **2013**, *8*, e70274. [CrossRef] [PubMed]
2. Jankovic, J. Parkinson's disease: Clinical features and diagnosis. *J. Neurol. Neurosurg. Psychiatry* **2008**, *79*, 368–376. [CrossRef]
3. Pellicano, C.; Benincasa, D.; Pisani, V.; Buttarelli, F.R.; Giovannelli, M.; Pontieri, F.E. Prodromal non-motor symptoms of Parkinson's disease. *Neuropsychiatr. Dis. Treat.* **2007**, *3*, 145–152. [CrossRef]
4. Schapira, A.H.V.; Chaudhuri, K.R.; Jenner, P. Non-motor features of Parkinson disease. *Nat. Rev. Neurosci.* **2017**, *18*, 509. [CrossRef]
5. Lawrence, V.; Pickett, J.; Ballard, C.; Murray, J. Patient and carer views on participating in clinical trials for prodromal Alzheimer's disease and mild cognitive impairment. *Int. J. Geriatr. Psychiatry* **2014**, *29*, 22–31. [CrossRef]
6. Mahlknecht, P.; Poewe, W. Pharmacotherapy for Disease Modification in Early Parkinson's Disease: How Early Should We Be? *J. Park. Dis.* **2024**, *14*, S407–S421. [CrossRef]
7. Iwatsubo, T. Development of disease-modifying therapies against Alzheimer's disease. *Psychiatry Clin. Neurosci.* **2024**, *78*, 491–494. [CrossRef] [PubMed]
8. Jenner, P.; Olanow, C.W. Oxidative stress and the pathogenesis of Parkinson's disease. *Neurology* **1996**, *47*, S161–S170. [CrossRef]
9. Dong-Chen, X.; Yong, C.; Yang, X.; Chen-Yu, S.; Li-Hua, P. Signaling pathways in Parkinson's disease: Molecular mechanisms and therapeutic interventions. *Signal Transduct. Target. Ther.* **2023**, *8*, 73. [CrossRef]
10. Wakabayashi, K.; Tanji, K.; Mori, F.; Takahashi, H. The Lewy body in Parkinson's disease: Molecules implicated in the formation and degradation of alpha-synuclein aggregates. *Neuropathology* **2007**, *27*, 494–506. [CrossRef] [PubMed]
11. Baba, M.; Nakajo, S.; Tu, P.H.; Tomita, T.; Nakaya, K.; Lee, V.M.; Trojanowski, J.Q.; Iwatsubo, T. Aggregation of alpha-synuclein in Lewy bodies of sporadic Parkinson's disease and dementia with Lewy bodies. *Am. J. Pathol.* **1998**, *152*, 879–884.
12. Ibarra-Gutierrez, M.T.; Serrano-Garcia, N.; Orozco-Ibarra, M. Rotenone-Induced Model of Parkinson's Disease: Beyond Mitochondrial Complex I Inhibition. *Mol. Neurobiol.* **2023**, *60*, 1929–1948. [CrossRef]
13. Bhurtel, S.; Katila, N.; Srivastav, S.; Neupane, S.; Choi, D.Y. Mechanistic comparison between MPTP and rotenone neurotoxicity in mice. *Neurotoxicology* **2019**, *71*, 113–121. [CrossRef] [PubMed]
14. Li, N.; Ragheb, K.; Lawler, G.; Sturgis, J.; Rajwa, B.; Melendez, J.A.; Robinson, J.P. Mitochondrial complex I inhibitor rotenone induces apoptosis through enhancing mitochondrial reactive oxygen species production. *J. Biol. Chem.* **2003**, *278*, 8516–8525. [CrossRef]
15. Yin, D.X.; Toyoda, H.; Nozaki, K.; Satoh, K.; Katagiri, A.; Adachi, K.; Kato, T.; Sato, H. Taste Impairments in a Parkinson's Disease Model Featuring Intranasal Rotenone Administration in Mice. *J. Park. Dis.* **2022**, *12*, 1863–1880. [CrossRef]
16. Cerri, S.; Blandini, F. In vivo modeling of prodromal stage of Parkinson's disease. *J. Neurosci. Methods* **2020**, *342*, 108801. [CrossRef]

17. Pun, P.B.; Lu, J.; Moochhala, S. Involvement of ROS in BBB dysfunction. *Free Radic. Res.* **2009**, *43*, 348–364. [CrossRef] [PubMed]
18. Chen, Y.; Dalwadi, G.; Benson, H.A. Drug delivery across the blood-brain barrier. *Curr. Drug Deliv.* **2004**, *1*, 361–376. [CrossRef]
19. Gopalakrishna, A.; Alexander, S.A. Understanding Parkinson Disease: A Complex and Multifaceted Illness. *J. Neurosci. Nurs.* **2015**, *47*, 320–326. [CrossRef] [PubMed]
20. Smith, Q.R. Transport of glutamate and other amino acids at the blood-brain barrier. *J. Nutr.* **2000**, *130*, 1016S–1022S. [CrossRef]
21. Begley, D.J. ABC transporters and the blood-brain barrier. *Curr. Pharm. Des.* **2004**, *10*, 1295–1312. [CrossRef]
22. Brightman, M.W.; Reese, T.S. Junctions between intimately apposed cell membranes in the vertebrate brain. *J. Cell Biol.* **1969**, *40*, 648–677. [CrossRef]
23. Stamatovic, S.M.; Keep, R.F.; Andjelkovic, A.V. Brain endothelial cell-cell junctions: How to "open" the blood brain barrier. *Curr. Neuropharmacol.* **2008**, *6*, 179–192. [CrossRef]
24. Chen, Y.; Liu, L. Modern methods for delivery of drugs across the blood-brain barrier. *Adv. Drug Deliv. Rev.* **2012**, *64*, 640–665. [CrossRef]
25. Meng, J.L.; Dong, Z.X.; Chen, Y.R.; Lin, M.H.; Liu, Y.C.; Roffler, S.R.; Lin, W.W.; Chang, C.Y.; Tzou, S.C.; Cheng, T.L.; et al. pH-Responsive Polyethylene Glycol Engagers for Enhanced Brain Delivery of PEGylated Nanomedicine to Treat Glioblastoma. *ACS Nano* **2025**, *19*, 307–321. [CrossRef]
26. Parodi, A.; Rudzinska, M.; Deviatkin, A.A.; Soond, S.M.; Baldin, A.V.; Zamyatnin, A.A., Jr. Established and Emerging Strategies for Drug Delivery Across the Blood-Brain Barrier in Brain Cancer. *Pharmaceutics* **2019**, *11*, 245. [CrossRef] [PubMed]
27. Chia, Y.C.; Anjum, C.E.; Yee, H.R.; Kenisi, Y.; Chan, M.K.S.; Wong, M.B.F.; Pan, S.Y. Stem Cell Therapy for Neurodegenerative Diseases: How Do Stem Cells Bypass the Blood-Brain Barrier and Home to the Brain? *Stem Cells Int.* **2020**, *2020*, 8889061. [CrossRef] [PubMed]
28. Zhou, Y.; Yamamoto, Y.; Xiao, Z.; Ochiya, T. The Immunomodulatory Functions of Mesenchymal Stromal/Stem Cells Mediated via Paracrine Activity. *J. Clin. Med.* **2019**, *8*, 1025. [CrossRef] [PubMed]
29. Pinho, A.G.; Cibrao, J.R.; Silva, N.A.; Monteiro, S.; Salgado, A.J. Cell Secretome: Basic Insights and Therapeutic Opportunities for CNS Disorders. *Pharmaceuticals* **2020**, *13*, 31. [CrossRef]
30. Joshi, J.M.; Muttigi, M.S.; Upadhya, R.; Seetharam, R.N. An overview of the current advances in the treatment of inflammatory diseases using mesenchymal stromal cell secretome. *Immunopharmacol. Immunotoxicol.* **2023**, *45*, 497–507. [CrossRef]
31. Saint-Pol, J.; Gosselet, F.; Duban-Deweer, S.; Pottiez, G.; Karamanos, Y. Targeting and Crossing the Blood-Brain Barrier with Extracellular Vesicles. *Cells* **2020**, *9*, 851. [CrossRef]
32. Ramos-Zaldivar, H.M.; Polakovicova, I.; Salas-Huenuleo, E.; Corvalan, A.H.; Kogan, M.J.; Yefi, C.P.; Andia, M.E. Extracellular vesicles through the blood-brain barrier: A review. *Fluids Barriers CNS* **2022**, *19*, 60. [CrossRef] [PubMed]
33. Matsumoto, J.; Stewart, T.; Banks, W.A.; Zhang, J. The Transport Mechanism of Extracellular Vesicles at the Blood-Brain Barrier. *Curr. Pharm. Des.* **2017**, *23*, 6206–6214. [CrossRef]
34. Dhuria, S.V.; Hanson, L.R.; Frey, W.H., 2nd. Intranasal delivery to the central nervous system: Mechanisms and experimental considerations. *J. Pharm. Sci.* **2010**, *99*, 1654–1673. [CrossRef]
35. Crowe, T.P.; Greenlee, M.H.W.; Kanthasamy, A.G.; Hsu, W.H. Mechanism of intranasal drug delivery directly to the brain. *Life Sci.* **2018**, *195*, 44–52. [CrossRef] [PubMed]
36. Ganger, S.; Schindowski, K. Tailoring Formulations for Intranasal Nose-to-Brain Delivery: A Review on Architecture, Physico-Chemical Characteristics and Mucociliary Clearance of the Nasal Olfactory Mucosa. *Pharmaceutics* **2018**, *10*, 116. [CrossRef]
37. Danielyan, L.; Beer-Hammer, S.; Stolzing, A.; Schafer, R.; Siegel, G.; Fabian, C.; Kahle, P.; Biedermann, T.; Lourhmati, A.; Buadze, M.; et al. Intranasal delivery of bone marrow-derived mesenchymal stem cells, macrophages, and microglia to the brain in mouse models of Alzheimer's and Parkinson's disease. *Cell Transplant.* **2014**, *23*, 123–139. [CrossRef]
38. Reitz, M.; Demestre, M.; Sedlacik, J.; Meissner, H.; Fiehler, J.; Kim, S.U.; Westphal, M.; Schmidt, N.O. Intranasal delivery of neural stem/progenitor cells: A noninvasive passage to target intracerebral glioma. *Stem Cells Transl. Med.* **2012**, *1*, 866–873. [CrossRef] [PubMed]
39. Kodali, M.; Castro, O.W.; Kim, D.K.; Thomas, A.; Shuai, B.; Attaluri, S.; Upadhya, R.; Gitai, D.; Madhu, L.N.; Prockop, D.J.; et al. Intranasally Administered Human MSC-Derived Extracellular Vesicles Pervasively Incorporate into Neurons and Microglia in both Intact and Status Epilepticus Injured Forebrain. *Int. J. Mol. Sci.* **2019**, *21*, 181. [CrossRef]
40. Battaglia, L.; Panciani, P.P.; Muntoni, E.; Capucchio, M.T.; Biasibetti, E.; De Bonis, P.; Mioletti, S.; Fontanella, M.; Swaminathan, S. Lipid nanoparticles for intranasal administration: Application to nose-to-brain delivery. *Expert Opin. Drug Deliv.* **2018**, *15*, 369–378. [CrossRef]
41. Agosti, E.; Zeppieri, M.; Antonietti, S.; Battaglia, L.; Ius, T.; Gagliano, C.; Fontanella, M.M.; Panciani, P.P. Navigating the Nose-to-Brain Route: A Systematic Review on Lipid-Based Nanocarriers for Central Nervous System Disorders. *Pharmaceutics* **2024**, *16*, 329. [CrossRef] [PubMed]

42. Stevens, J.; Ploeger, B.A.; van der Graaf, P.H.; Danhof, M.; de Lange, E.C. Systemic and direct nose-to-brain transport pharmacokinetic model for remoxipride after intravenous and intranasal administration. *Drug Metab. Dispos.* **2011**, *39*, 2275–2282. [CrossRef] [PubMed]
43. Christodoulou, I.; Kolisis, F.N.; Papaevangeliou, D.; Zoumpourlis, V. Comparative Evaluation of Human Mesenchymal Stem Cells of Fetal (Wharton's Jelly) and Adult (Adipose Tissue) Origin during Prolonged In Vitro Expansion: Considerations for Cytotherapy. *Stem Cells Int.* **2013**, *2013*, 246134. [CrossRef]
44. Zhao, Q.; Ren, H.; Li, X.; Chen, Z.; Zhang, X.; Gong, W.; Liu, Y.; Pang, T.; Han, Z.C. Differentiation of human umbilical cord mesenchymal stromal cells into low immunogenic hepatocyte-like cells. *Cytotherapy* **2009**, *11*, 414–426. [CrossRef]
45. Xiang, E.; Han, B.; Zhang, Q.; Rao, W.; Wang, Z.; Chang, C.; Zhang, Y.; Tu, C.; Li, C.; Wu, D. Human umbilical cord-derived mesenchymal stem cells prevent the progression of early diabetic nephropathy through inhibiting inflammation and fibrosis. *Stem Cell Res. Ther.* **2020**, *11*, 336. [CrossRef] [PubMed]
46. Wang, J.; Hu, W.; Feng, Z.; Feng, M. BDNF-overexpressing human umbilical cord mesenchymal stem cell-derived motor neurons improve motor function and prolong survival in amyotrophic lateral sclerosis mice. *Neurol. Res.* **2021**, *43*, 199–209. [CrossRef]
47. Sun, Z.; Gu, P.; Xu, H.; Zhao, W.; Zhou, Y.; Zhou, L.; Zhang, Z.; Wang, W.; Han, R.; Chai, X.; et al. Human Umbilical Cord Mesenchymal Stem Cells Improve Locomotor Function in Parkinson's Disease Mouse Model Through Regulating Intestinal Microorganisms. *Front. Cell Dev. Biol.* **2021**, *9*, 808905. [CrossRef]
48. Oppliger, B.; Joerger-Messerli, M.; Mueller, M.; Reinhart, U.; Schneider, P.; Surbek, D.V.; Schoeberlein, A. Intranasal Delivery of Umbilical Cord-Derived Mesenchymal Stem Cells Preserves Myelination in Perinatal Brain Damage. *Stem Cells Dev.* **2016**, *25*, 1234–1242. [CrossRef]
49. Zhang, Z.; He, S.; Jiang, W.; Lu, J.; Liu, S.; Xu, W.; Wang, Z.; Lu, F.; Xiao, Q.; Zhang, J. Uptake of Mesenchymal Stem Cell-Derived Exosomes in Mouse Brain through Intranasal Delivery. *Curr. Drug Deliv.* **2024**, *22*, 1112–1124. [CrossRef]
50. Balyasnikova, I.V.; Prasol, M.S.; Ferguson, S.D.; Han, Y.; Ahmed, A.U.; Gutova, M.; Tobias, A.L.; Mustafi, D.; Rincon, E.; Zhang, L.; et al. Intranasal delivery of mesenchymal stem cells significantly extends survival of irradiated mice with experimental brain tumors. *Mol. Ther.* **2014**, *22*, 140–148. [CrossRef]
51. Donega, V.; van Velthoven, C.T.; Nijboer, C.H.; van Bel, F.; Kas, M.J.; Kavelaars, A.; Heijnen, C.J. Intranasal mesenchymal stem cell treatment for neonatal brain damage: Long-term cognitive and sensorimotor improvement. *PLoS ONE* **2013**, *8*, e51253. [CrossRef]
52. Ma, X.; Huang, M.; Zheng, M.; Dai, C.; Song, Q.; Zhang, Q.; Li, Q.; Gu, X.; Chen, H.; Jiang, G.; et al. ADSCs-derived extracellular vesicles alleviate neuronal damage, promote neurogenesis and rescue memory loss in mice with Alzheimer's disease. *J. Control. Release* **2020**, *327*, 688–702. [CrossRef] [PubMed]
53. Qin, Q.; Shan, Z.; Xing, L.; Jiang, Y.; Li, M.; Fan, L.; Zeng, X.; Ma, X.; Zheng, D.; Wang, H.; et al. Synergistic effect of mesenchymal stem cell-derived extracellular vesicle and miR-137 alleviates autism-like behaviors by modulating the NF-kappaB pathway. *J. Transl. Med.* **2024**, *22*, 446. [CrossRef] [PubMed]
54. Donega, V.; Nijboer, C.H.; van Tilborg, G.; Dijkhuizen, R.M.; Kavelaars, A.; Heijnen, C.J. Intranasally administered mesenchymal stem cells promote a regenerative niche for repair of neonatal ischemic brain injury. *Exp. Neurol.* **2014**, *261*, 53–64. [CrossRef] [PubMed]
55. O'Connor, J.C.; Lawson, M.A.; Andre, C.; Moreau, M.; Lestage, J.; Castanon, N.; Kelley, K.W.; Dantzer, R. Lipopolysaccharide-induced depressive-like behavior is mediated by indoleamine 2,3-dioxygenase activation in mice. *Mol. Psychiatry* **2009**, *14*, 511–522. [CrossRef]
56. Mayorga, A.J.; Lucki, I. Limitations on the use of the C57BL/6 mouse in the tail suspension test. *Psychopharmacology* **2001**, *155*, 110–112. [CrossRef]
57. Dunn, A.J.; Swiergiel, A.H. Effects of interleukin-1 and endotoxin in the forced swim and tail suspension tests in mice. *Pharmacol. Biochem. Behav.* **2005**, *81*, 688–693. [CrossRef]
58. Can, A.; Dao, D.T.; Arad, M.; Terrillion, C.E.; Piantadosi, S.C.; Gould, T.D. The mouse forced swim test. *J. Vis. Exp.* **2012**, *59*, 3638. [CrossRef]
59. Dang, H.; Chen, Y.; Liu, X.; Wang, Q.; Wang, L.; Jia, W.; Wang, Y. Antidepressant effects of ginseng total saponins in the forced swimming test and chronic mild stress models of depression. *Prog. Neuropsychopharmacol. Biol. Psychiatry* **2009**, *33*, 1417–1424. [CrossRef]
60. Yankelevitch-Yahav, R.; Franko, M.; Huly, A.; Doron, R. The forced swim test as a model of depressive-like behavior. *J. Vis. Exp.* **2015**, *97*, 52587. [CrossRef]
61. Fleming, S.M.; Tetreault, N.A.; Mulligan, C.K.; Hutson, C.B.; Masliah, E.; Chesselet, M.F. Olfactory deficits in mice overexpressing human wildtype alpha-synuclein. *Eur. J. Neurosci.* **2008**, *28*, 247–256. [CrossRef] [PubMed]
62. Fleming, S.M.; Mulligan, C.K.; Richter, F.; Mortazavi, F.; Lemesre, V.; Frias, C.; Zhu, C.; Stewart, A.; Gozes, I.; Morimoto, B.; et al. A pilot trial of the microtubule-interacting peptide (NAP) in mice overexpressing alpha-synuclein shows improvement in motor function and reduction of alpha-synuclein inclusions. *Mol. Cell Neurosci.* **2011**, *46*, 597–606. [CrossRef] [PubMed]

63. Nathan, B.P.; Yost, J.; Litherland, M.T.; Struble, R.G.; Switzer, P.V. Olfactory function in apoE knockout mice. *Behav. Brain Res.* **2004**, *150*, 1–7. [CrossRef]
64. Hutter-Saunders, J.A.; Gendelman, H.E.; Mosley, R.L. Murine motor and behavior functional evaluations for acute 1-methyl-4-phenyl-1,2,3,6-tetrahydropyridine (MPTP) intoxication. *J. Neuroimmune Pharmacol.* **2012**, *7*, 279–288. [CrossRef]
65. Crestani, F.; Martin, J.R.; Mohler, H.; Rudolph, U. Resolving differences in GABAA receptor mutant mouse studies. *Nat. Neurosci.* **2000**, *3*, 1059. [CrossRef]
66. Tao-Cheng, J.H.; Gallant, P.E.; Brightman, M.W.; Dosemeci, A.; Reese, T.S. Structural changes at synapses after delayed perfusion fixation in different regions of the mouse brain. *J. Comp. Neurol.* **2007**, *501*, 731–740. [CrossRef]
67. Rosenberg, G.A.; Cunningham, L.A.; Wallace, J.; Alexander, S.; Estrada, E.Y.; Grossetete, M.; Razhagi, A.; Miller, K.; Gearing, A. Immunohistochemistry of matrix metalloproteinases in reperfusion injury to rat brain: Activation of MMP-9 linked to stromelysin-1 and microglia in cell cultures. *Brain Res.* **2001**, *893*, 104–112. [CrossRef]
68. Valley, M.T.; Mullen, T.R.; Schultz, L.C.; Sagdullaev, B.T.; Firestein, S. Ablation of mouse adult neurogenesis alters olfactory bulb structure and olfactory fear conditioning. *Front. Neurosci.* **2009**, *3*, 51. [CrossRef]
69. Syrbu, S.I.; Cohen, M.B. An enhanced antigen-retrieval protocol for immunohistochemical staining of formalin-fixed, paraffin-embedded tissues. *Methods Mol. Biol.* **2011**, *717*, 101–110. [CrossRef]
70. He, J.; Deng, L.; Liu, H.; Chen, T.; Chen, S.; Xia, S.; Liu, Y. BCL2L10/BECN1 modulates hepatoma cells autophagy by regulating PI3K/AKT signaling pathway. *Aging* **2019**, *11*, 350–370. [CrossRef] [PubMed]
71. Moon, S.H.; Kwon, Y.; Huh, Y.E.; Choi, H.J. Trehalose ameliorates prodromal non-motor deficits and aberrant protein accumulation in a rotenone-induced mouse model of Parkinson's disease. *Arch. Pharm. Res.* **2022**, *45*, 417–432. [CrossRef]
72. Li, S.; Li, W.; Wu, X.; Li, J.; Yang, J.; Tu, C.; Ye, X.; Ling, S. Olfactory deficit is associated with mitral cell dysfunction in the olfactory bulb of P301S tau transgenic mice. *Brain Res. Bull.* **2019**, *148*, 34–45. [CrossRef]
73. Gardner, B.; Dieriks, B.V.; Cameron, S.; Mendis, L.H.S.; Turner, C.; Faull, R.L.M.; Curtis, M.A. Metal concentrations and distributions in the human olfactory bulb in Parkinson's disease. *Sci. Rep.* **2017**, *7*, 10454. [CrossRef] [PubMed]
74. Huisman, E.; Uylings, H.B.; Hoogland, P.V. A 100% increase of dopaminergic cells in the olfactory bulb may explain hyposmia in Parkinson's disease. *Mov. Disord.* **2004**, *19*, 687–692. [CrossRef] [PubMed]
75. Zhang, Z.; Du, X.; Xu, H.; Xie, J.; Jiang, H. Lesion of medullary catecholaminergic neurons is associated with cardiovascular dysfunction in rotenone-induced Parkinson's disease rats. *Eur. J. Neurosci.* **2015**, *42*, 2346–2355. [CrossRef]
76. Bernheimer, H.; Birkmayer, W.; Hornykiewicz, O.; Jellinger, K.; Seitelberger, F. Brain dopamine and the syndromes of Parkinson and Huntington. Clinical, morphological and neurochemical correlations. *J. Neurol. Sci.* **1973**, *20*, 415–455. [CrossRef] [PubMed]
77. Fullard, M.E.; Morley, J.F.; Duda, J.E. Olfactory Dysfunction as an Early Biomarker in Parkinson's Disease. *Neurosci. Bull.* **2017**, *33*, 515–525. [CrossRef]
78. Ravina, B.; Camicioli, R.; Como, P.G.; Marsh, L.; Jankovic, J.; Weintraub, D.; Elm, J. The impact of depressive symptoms in early Parkinson disease. *Neurology* **2007**, *69*, 342–347. [CrossRef]
79. Chatterjee, M.; Jaiswal, M.; Palit, G. Comparative evaluation of forced swim test and tail suspension test as models of negative symptom of schizophrenia in rodents. *ISRN Psychiatry* **2012**, *2012*, 595141. [CrossRef]
80. Solich, J.; Palach, P.; Budziszewska, B.; Dziedzicka-Wasylewska, M. Effect of two behavioral tests on corticosterone level in plasma of mice lacking the noradrenaline transporter. *Pharmacol. Rep.* **2008**, *60*, 1008–1013. [CrossRef]
81. Li, Y.H.; Feng, L.; Zhang, G.X.; Ma, C.G. Intranasal delivery of stem cells as therapy for central nervous system disease. *Exp. Mol. Pathol.* **2015**, *98*, 145–151. [CrossRef] [PubMed]
82. Yu-Taeger, L.; Stricker-Shaver, J.; Arnold, K.; Bambynek-Dziuk, P.; Novati, A.; Singer, E.; Lourhmati, A.; Fabian, C.; Magg, J.; Riess, O.; et al. Intranasal Administration of Mesenchymal Stem Cells Ameliorates the Abnormal Dopamine Transmission System and Inflammatory Reaction in the R6/2 Mouse Model of Huntington Disease. *Cells* **2019**, *8*, 595. [CrossRef] [PubMed]
83. Salama, M.; Sobh, M.; Emam, M.; Abdalla, A.; Sabry, D.; El-Gamal, M.; Lotfy, A.; El-Husseiny, M.; Sobh, M.; Shalash, A.; et al. Effect of intranasal stem cell administration on the nigrostriatal system in a mouse model of Parkinson's disease. *Exp. Ther. Med.* **2017**, *13*, 976–982. [CrossRef]
84. Losurdo, M.; Pedrazzoli, M.; D'Agostino, C.; Elia, C.A.; Massenzio, F.; Lonati, E.; Mauri, M.; Rizzi, L.; Molteni, L.; Bresciani, E.; et al. Intranasal delivery of mesenchymal stem cell-derived extracellular vesicles exerts immunomodulatory and neuroprotective effects in a 3xTg model of Alzheimer's disease. *Stem Cells Transl. Med.* **2020**, *9*, 1068–1084. [CrossRef]
85. Heris, R.M.; Shirvaliloo, M.; Abbaspour-Aghdam, S.; Hazrati, A.; Shariati, A.; Youshanlouei, H.R.; Niaragh, F.J.; Valizadeh, H.; Ahmadi, M. The potential use of mesenchymal stem cells and their exosomes in Parkinson's disease treatment. *Stem Cell Res. Ther.* **2022**, *13*, 371. [CrossRef]
86. Xilouri, M.; Brekk, O.R.; Stefanis, L. Autophagy and Alpha-Synuclein: Relevance to Parkinson's Disease and Related Synucleopathies. *Mov. Disord.* **2016**, *31*, 178–192. [CrossRef]
87. Porritt, M.J.; Batchelor, P.E.; Hughes, A.J.; Kalnins, R.; Donnan, G.A.; Howells, D.W. New dopaminergic neurons in Parkinson's disease striatum. *Lancet* **2000**, *356*, 44–45. [CrossRef]

88. Song, D.D.; Haber, S.N. Striatal responses to partial dopaminergic lesion: Evidence for compensatory sprouting. *J. Neurosci.* **2000**, *20*, 5102–5114. [CrossRef]
89. Doty, R.L.; Risser, J.M. Influence of the D-2 dopamine receptor agonist quinpirole on the odor detection performance of rats before and after spiperone administration. *Psychopharmacology* **1989**, *98*, 310–315. [CrossRef]
90. Duchamp-Viret, P.; Coronas, V.; Delaleu, J.C.; Moyse, E.; Duchamp, A. Dopaminergic modulation of mitral cell activity in the frog olfactory bulb: A combined radioligand binding-electrophysiological study. *Neuroscience* **1997**, *79*, 203–216. [CrossRef] [PubMed]
91. Dang, S.; Xu, H.; Xu, C.; Cai, W.; Li, Q.; Cheng, Y.; Jin, M.; Wang, R.X.; Peng, Y.; Zhang, Y.; et al. Autophagy regulates the therapeutic potential of mesenchymal stem cells in experimental autoimmune encephalomyelitis. *Autophagy* **2014**, *10*, 1301–1315. [CrossRef]
92. Galleu, A.; Riffo-Vasquez, Y.; Trento, C.; Lomas, C.; Dolcetti, L.; Cheung, T.S.; von Bonin, M.; Barbieri, L.; Halai, K.; Ward, S.; et al. Apoptosis in mesenchymal stromal cells induces in vivo recipient-mediated immunomodulation. *Sci. Transl. Med.* **2017**, *9*, eaam7828. [CrossRef]
93. Yang, B.; Duan, W.; Wei, L.; Zhao, Y.; Han, Z.; Wang, J.; Wang, M.; Dai, C.; Zhang, B.; Chen, D.; et al. Bone Marrow Mesenchymal Stem Cell-Derived Hepatocyte-like Cell Exosomes Reduce Hepatic Ischemia/Reperfusion Injury by Enhancing Autophagy. *Stem. Cells Dev.* **2020**, *29*, 372–379. [CrossRef]
94. Kou, M.; Huang, L.; Yang, J.; Chiang, Z.; Chen, S.; Liu, J.; Guo, L.; Zhang, X.; Zhou, X.; Xu, X.; et al. Mesenchymal stem cell-derived extracellular vesicles for immunomodulation and regeneration: A next generation therapeutic tool? *Cell Death Dis.* **2022**, *13*, 580. [CrossRef]
95. Seo, Y.; Kim, H.S.; Hong, I.S. Stem Cell-Derived Extracellular Vesicles as Immunomodulatory Therapeutics. *Stem Cells Int.* **2019**, *2019*, 5126156. [CrossRef]
96. Cai, J.; Wu, J.; Wang, J.; Li, Y.; Hu, X.; Luo, S.; Xiang, D. Extracellular vesicles derived from different sources of mesenchymal stem cells: Therapeutic effects and translational potential. *Cell Biosci.* **2020**, *10*, 69. [CrossRef]
97. Lo Cicero, A.; Delevoye, C.; Gilles-Marsens, F.; Loew, D.; Dingli, F.; Guere, C.; Andre, N.; Vie, K.; van Niel, G.; Raposo, G. Exosomes released by keratinocytes modulate melanocyte pigmentation. *Nat. Commun.* **2015**, *6*, 7506. [CrossRef]
98. Rani, S.; Ryan, A.E.; Griffin, M.D.; Ritter, T. Mesenchymal Stem Cell-derived Extracellular Vesicles: Toward Cell-free Therapeutic Applications. *Mol. Ther.* **2015**, *23*, 812–823. [CrossRef] [PubMed]
99. Jaimes, Y.; Naaldijk, Y.; Wenk, K.; Leovsky, C.; Emmrich, F. Mesenchymal Stem Cell-Derived Microvesicles Modulate Lipopolysaccharides-Induced Inflammatory Responses to Microglia Cells. *Stem Cells* **2017**, *35*, 812–823. [CrossRef] [PubMed]
100. Quan, J.; Liu, Q.; Li, P.; Yang, Z.; Zhang, Y.; Zhao, F.; Zhu, G. Mesenchymal stem cell exosome therapy: Current research status in the treatment of neurodegenerative diseases and the possibility of reversing normal brain aging. *Stem Cell Res. Ther.* **2025**, *16*, 76. [CrossRef] [PubMed]
101. Aguilera, Y.; Mellado-Damas, N.; Olmedo-Moreno, L.; Lopez, V.; Panadero-Moron, C.; Benito, M.; Guerrero-Cazares, H.; Marquez-Vega, C.; Martin-Montalvo, A.; Capilla-Gonzalez, V. Preclinical Safety Evaluation of Intranasally Delivered Human Mesenchymal Stem Cells in Juvenile Mice. *Cancers* **2021**, *13*, 1169. [CrossRef] [PubMed]
102. Hwang, J.W.; Lee, N.K.; Yang, J.H.; Son, H.J.; Bang, S.I.; Chang, J.W.; Na, D.L. A Comparison of Immune Responses Exerted Following Syngeneic, Allogeneic, and Xenogeneic Transplantation of Mesenchymal Stem Cells into the Mouse Brain. *Int. J. Mol. Sci.* **2020**, *21*, 3052. [CrossRef] [PubMed]